

ARTICLE **OPEN**

Senescent cancer cell-derived nanovesicle as a personalized therapeutic cancer vaccine

Jihye Hong¹, Mungyo Jung², Cheesue Kim², Mikyung Kang¹, Seokhyeong Go¹, Heesu Sohn², Sangjun Moon², Sungpil Kwon², Seuk Young Song² and Byung-Soo Kim^{1,2,3}✉

© The Author(s) 2023

The development of therapeutic cancer vaccines (TCVs) that provide clinical benefits is challenging mainly due to difficulties in identifying immunogenic tumor antigens and effectively inducing antitumor immunity. Furthermore, there is an urgent need for personalized TCVs because only a limited number of tumor antigens are shared among cancer patients. Several autologous nanovaccines that do not require the identification of immunogenic tumor antigens have been proposed as personalized TCVs. However, these nanovaccines generally require exogenous adjuvants (e.g., Toll-like receptor agonists) to improve vaccine immunogenicity, which raises safety concerns. Here, we present senescent cancer cell-derived nanovesicle (SCCNV) as a personalized TCV that provides patient-specific tumor antigens and improved vaccine immunogenicity without the use of exogenous adjuvants. SCCNVs are prepared by inducing senescence in cancer cells *ex vivo* and subsequently extruding the senescent cancer cells through nanoporous membranes. In the clinical setting, SCCNVs can be prepared from autologous cancer cells from the blood of liquid tumor patients or from tumors surgically removed from solid cancer patients. SCCNVs also contain interferon- γ and tumor necrosis factor- α , which are expressed during senescence. These endogenous cytokines act as adjuvants and enhance vaccine immunogenicity, avoiding the need for exogenous adjuvants. Intradermally injected SCCNVs effectively activate dendritic cells and tumor-specific T cells and inhibit primary and metastatic tumor growth and tumor recurrence. SCCNV therapy showed an efficacy similar to that of immune checkpoint blockade (ICB) therapy and synergized with ICB. SCCNVs, which can be prepared using a simple and facile procedure, show potential as personalized TCVs.

Experimental & Molecular Medicine (2023) 55:541–554; <https://doi.org/10.1038/s12276-023-00951-z>

INTRODUCTION

Cancer immunotherapies, such as immune checkpoint blockade therapy and chimeric antigen receptor T (CAR-T) cell therapy, activate antitumor immunity in cancer patients and have shown significant success in clinical oncology^{1–4}. Therapeutic cancer vaccines (TCVs), another cancer immunotherapy approach, involve the administration of immunogenic tumor antigens to stimulate the patient adaptive immune system against the tumor⁵. However, the development of clinically applicable TCVs has been limited thus far. A tumor antigen-loaded DC-based TCV (Sipuleucel-T) was approved by the FDA in 2010 to treat prostate cancer⁶, but no further TCVs have been approved. The difficulties associated with the identification of immunogenic tumor antigens and insufficient antitumor immunity of TCVs are the main limitations in the development of clinically applicable TCVs⁷.

A key step in the TCV development process is the identification of immunogenic tumor antigens that elicit antitumor immunity. Various tumor-associated antigens (TAAs) have been suggested as new target antigens for TCVs, including human epidermal growth factor receptor-2 (HER-2) and mesothelin and melanoma-associated antigen recognized by T cells (MART-1)^{8,9}. Recently, neoantigens, which are nonself antigens that are expressed in

only mutated cancer cells, have emerged as new target antigens for TCVs. Neoantigens can be profiled by next-generation sequencing-based cancer exome sequencing^{10,11}. However, most TCVs employing TAAs or neoantigens have failed to achieve therapeutic benefit in clinical trials^{12,13}.

The disappointing clinical results for TCVs employing TAAs are mainly due to the nonexclusive and heterogeneous expression of TAAs in tumor tissues¹⁰. TAAs are also expressed in normal tissues, resulting in off-target side effects mediated by activated T cells or elimination of TAA-specific T cells through immune tolerance. In addition, the heterogeneous expression of TAAs in tumors leads to low effectiveness in the vaccine-mediated killing of tumors.

Meanwhile, neoantigens are highly individual specific, and only a small number of neoantigens are shared among cancer patients¹⁰. This demands the development of personalized TCVs. Recently, next-generation sequencing technology and whole-genome mapping have made it feasible to identify patient-specific neoantigens and design personalized TCVs¹⁴. However, most of the discovered neoantigens exhibit low immunogenicity or low affinity for major histocompatibility complex (MHC) molecules. Profiling of cancer patients has revealed that only a small fraction (~1–2%) of neoantigens in cancer cells are recognized by T cells

¹Interdisciplinary Program for Bioengineering, Seoul National University, Seoul 08826, Republic of Korea. ²School of Chemical and Biological Engineering, Seoul National University, Seoul 08826, Republic of Korea. ³Institute of Chemical Processes, Institute of Engineering Research, BioMAX, Seoul National University, Seoul 08826, Republic of Korea. ✉email: byungskim@snu.ac.kr

and induce sufficient immune responses¹⁵. In addition, some neoantigens often disappear in tumor tissues due to the rapid mutation rate in tumor cells. This poses a problem for the development of patient-specific neoantigen TCVs.

Nanovaccines made of autologous cancer cell membranes have been proposed as personalized TCVs that do not require the identification of immunogenic tumor antigens^{16,17}. However, inducing sufficient antitumor immune responses *in vivo* often requires the addition of an appropriate exogenous adjuvant that induces dendritic cell (DC) activation¹⁸, and nanovaccines made of autologous cancer cell membranes generally require exogenous adjuvants (e.g., TLR agonists) to improve vaccine immunogenicity. These adjuvants include CpG oligodeoxynucleotides (CpG ODNs), resiquimod (R848), and polyinosinic:polycytidylic acid (poly I:C)^{19,20}. However, these TLR agonists raise safety concerns due to the potential to cause severe adverse effects^{21,22}. Thus, the use of safe and effective adjuvants is required to achieve safe and effective TCV therapy.

Here, we present senescence-induced cancer cell-derived nanovesicle (SCCNV) as a personalized TCV that can overcome the limitations of current TCVs. Nanovesicles are exosome-mimetic nanosized vesicles produced by extruding cells through nanoporous membranes²³. Nanovesicles can deliver RNAs and proteins originating from parental cells and exhibit a higher production efficiency than naturally secreted exosomes^{23,24}. Nanovesicles derived from various immune cells, including T cells, macrophages and dendritic cells, have been explored for cancer immunotherapy^{24–26}. SCCNVs were produced by serial extrusion of senescence-induced cancer cells (Fig. 1a). Autologous cancer cells for SCCNV preparation would be clinically available from cancer patients, and SCCNVs prepared from autologous cancer cells can deliver a variety of patient-specific tumor antigens, avoiding the complicated process of neoantigen identification. While TCVs with a single TAA or neoantigen may face immune escape that is caused by the ceaseless mutation of cancer cells *in vivo*, SCCNVs that would contain a spectrum of tumor antigens may avoid the immune escape problem. Cellular senescence is a phenomenon characterized by arrest during cell division in response to various cellular stresses, such as DNA damage and oxidative stress²⁷. Senescent cells exhibit a senescence-associated secretory phenotype (SASP), which includes expression of interferon-gamma (IFN- γ) and tumor necrosis factor-alpha (TNF- α)²⁸. In the present study, IFN- γ and TNF- α were expressed during *ex vivo* senescence induction and contained in SCCNVs. These endogenous cytokines served as adjuvants that enhance the immunogenicity of the vaccine. These endogenous adjuvants would be safer than conventional exogenous adjuvants, such as MPLA, poly I:C and CpG, which may have safety concerns^{21,22}. Intradermally injected SCCNVs could deliver tumor antigens and adjuvants (IFN- γ and TNF- α) to DCs, resulting in DC activation, DC migration to the draining lymph nodes, and activation of tumor-specific T cells capable of cancer cell killing (Fig. 1b).

EXPERIMENTAL SECTION

Experimental animals

All animal experiments were approved by the Institutional Animal Care and Use Committee (IACUC) of Seoul National University (SNU-200630-2-4) and performed in compliance with the guidelines of the IACUC. For *in vivo* studies, six-week-old C57BL/6 mice and six-week-old B/C mice were purchased from Orient Bio (Gyeonggi, Korea) or JA Bio (Gyeonggi, Korea).

Cell culture

B16F10 cells were purchased from American Type Culture Collection (ATCC; VA, USA) and were cultured in Dulbecco's modified Eagle's medium (DMEM; Gibco, NY, USA) supplemented with 10% (v/v) FBS and 1% (v/v) PS. E.G7-OVA cells, a variant of the

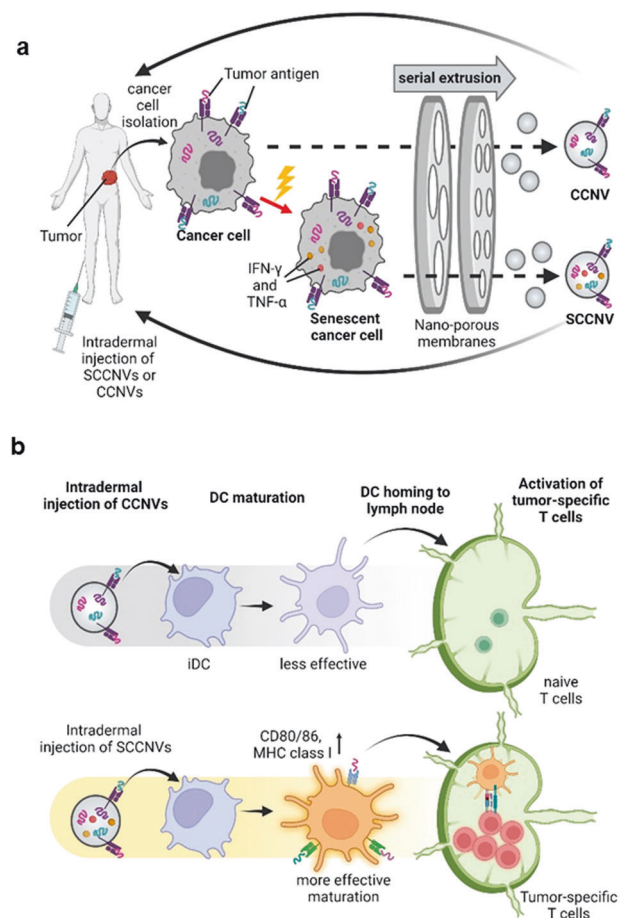


Fig. 1 Experimental scheme of SCCNVs. Illustration of (a) SCCNV preparation and personalized cancer vaccination and (b) the proposed mode of action of the vaccines. SCCNV senescent cancer cell-derived nanovesicle, CCNV cancer cell-derived nanovesicle, iDC immature dendritic cell, mDC mature dendritic cell.

EL4 cell line that expresses full-length OVA, were a gift from Professor Junsang Doh, Seoul National University, Seoul, Korea. E.G7-OVA cells were cultured in RPMI 1640 medium (Gibco) containing 10% (v/v) FBS, 1% (v/v) PS, 10 mM HEPES, 1.0 mM sodium pyruvate, 0.05 mM β -mercaptoethanol and 0.04 μ g/ml G-418 antibiotics (Roche). 4T1 cells were purchased from ATCC and cultured in RPMI 1640 medium containing 10% (v/v) FBS and 1% (v/v) PS. Primary T cells were isolated from the spleen of 6-week-old female C57BL/6 mice (Orient Bio, Gyeonggi, Korea) using the MojoSort™ Mouse CD8 T Cell Isolation Kit (BioLegend) according to the manufacturer's protocol. Cells were then cultured in RPMI 1640 medium supplemented with 10% (v/v) FBS, 1% (v/v) PS, 1% (v/v) GlutaMAX (Gibco), 10 mM HEPES, 1 mM sodium pyruvate and 55 μ M 2-mercaptoethanol.

Preparation of SCCNVs

SCCNVs were produced from cancer cell lines. For senescence induction, 0.1 μ M doxorubicin hydrochloride (doxorubicin HCl; Sigma-Aldrich, MO, USA) was added to the cell culture medium for 24 h. Then, the cells were washed with PBS, changed to doxorubicin-free medium and cultured for an additional 4 days^{29,30}. Senescence-induced cancer cells were detached from the cell culture plate using trypsin-EDTA, washed with PBS and serially extruded through polycarbonate membrane filters (Whatman, UK) with pore sizes of 1 μ m, 400 nm and 200 nm using a mini-extruder (Avanti Polar Lipids, AL, USA) to obtain nanovesicles as previously reported²³. To reload antigen peptides that might

have been dissociated from the MHC class I molecules on nanovesicles onto the MHC class I molecules, the pH of the nanovesicle-containing solution was adjusted to 5.5 with sodium acetate buffer for 30 min and then neutralized with Tris-HCl buffer^{31,32}. The nanovesicles were then centrifuged at 30,000 × *g* for 1 h at 4 °C. The protein concentration of isolated SCCNVs was quantified using Bradford reagent (Sigma–Aldrich) according to the manufacturer’s protocol.

Optimization of senescence induction

B16F10 cells were treated with doxorubicin HCl at concentrations of 0, 0.1, 0.5, and 1 μM. To evaluate senescence, the cells were stained with a senescence-associated β-galactosidase (SA-β-gal) staining kit (Cell Signaling Technology, MA, USA) according to the manufacturer’s protocol. To evaluate the cytotoxicity of doxorubicin HCl, Cell Counting Kit-8 (CCK-8; DoGenBio, Seoul, Korea) was used according to the manufacturer’s protocol.

Characterization of SCCNVs

The size distributions of SCCNVs were assessed using dynamic light scattering (Zetasizer Nano ZS, Malvern Panalytical, UK). To evaluate the colloidal stability of SCCNVs in a 30% FBS-containing buffer, the hydrodynamic diameter of SCCNVs was detected with a Zetasizer at various time points. The morphology of SCCNVs was evaluated with a JEM-2100 transmission electron microscope (JEOL, Japan) installed at the National Center for Inter-university Research Facilities (NCIRF) at Seoul National University. The relative mRNA expression levels of IFN-γ and TNF-α were determined with qRT–PCR analysis. mRNA was extracted from cancer cells or nanovesicles using QIAzol Lysis Reagent (Qiagen, CA, USA). RNA from each group was used for cDNA synthesis using PCR PreMix (Bioneer, Daejeon, Korea). SYBR green-based qRT–PCR was performed with TOPreal™ qPCR 2X PreMIX (Enzynomics, Daejeon, Korea). The cycling conditions were as follows: initial denaturation at 95 °C for 15 min, followed by 60 cycles at 95 °C for 10 s, 60 °C for 15 s and 72 °C for 30 s. The expression of each gene was normalized to that of GAPDH. The protein levels of IFN-γ and TNF-α were evaluated by western blotting using an anti-mouse IFN-γ antibody, anti-mouse TNF-α antibody (Bioss, MA, USA) and anti-mouse GAPDH antibody (Invitrogen, CA, USA). GAPDH was used as the control protein. For Coomassie blue staining, the proteins in lysates generated from normal B16F10 cells, senescent B16F10 cells, CCNVs and SCCNVs were separated using SDS–PAGE, and the polyacrylamide gel was stained with Coomassie blue using PageBlue™ Protein Staining Solution (Thermo Scientific, MA, USA) to visualize the proteins. The amounts of IFN-γ and TNF-α were detected by analyzing lysates generated from CCNVs and SCCNVs with an ELISA kit (BioLegend). The calculated amounts of IFN-γ and TNF-α were divided by the total protein amount to obtain the amounts of IFN-γ and TNF-α per 1 μg of SCCNVs.

Isolation of BMDCs

BMDCs were isolated as previously described³³. Briefly, 6-week-old C57BL/6 mice were sacrificed, and the femurs were isolated from the hind limbs. The bones were flushed with PBS using syringes to isolate bone marrow cells. Red blood cell lysis buffer was added. After centrifugation, mononuclear bone marrow cells were cultured in dishes containing 10 mL of differentiation medium consisting of RPMI 1640 medium supplemented with 20 ng/mL GM-CSF (R&D Systems, MN, USA) and 10% (v/v) FBS. After 3 days, 5 mL of fresh differentiation medium was added to the dishes. Differentiated BMDCs were collected on Day 10.

In vitro DC maturation

For in vitro DC maturation analysis, 5 × 10⁵ BMDCs were plated in each well of 6-well plates prior to SCCNV treatment. To investigate SCCNV uptake by DCs, 20 μg of CCNVs or SCCNVs was stained with 1,1'-dioctadecyl-3,3,3',3'-tetramethylindocarbocyanine perchlorate

(Dil, Invitrogen) according to the manufacturer’s protocol. BMDCs were treated with Dil-stained CCNVs or SCCNVs and analyzed by FACS using a BD Canto-II flow cytometer (BD Sciences, CA, USA). To determine mRNA levels in DCs, BMDCs were treated with 20 μg of CCNVs or SCCNVs for 4 h. Treatment with 100 ng/ml lipopolysaccharide (LPS; Sigma–Aldrich, MO, USA) was used as the positive control. Then, the cells were lysed with QIAzol lysis reagent (Qiagen, CA, USA) for mRNA extraction. The relative mRNA levels of IL-6, IL-12p40 and CCR7 were evaluated by qRT–PCR. The expression of each gene was normalized to that of GAPDH. For detection of surface protein expression on BMDCs, BMDCs were treated with 20 μg of CCNVs or SCCNVs for 24 h. Then, the BMDCs were detached with trypsin-EDTA and stained with the following antibodies: APC–Cy7 anti-mouse CD11c antibody, PE anti-mouse CD80 antibody, APC anti-mouse CD86 antibody and FITC anti-mouse MHC class I antibody (BioLegend, CA, USA). Fluorescently labeled DCs were analyzed with a BD Canto-II flow cytometer (BD Sciences). FACS data were analyzed using FlowJo software (TreeStar Inc., OR, USA). For proinflammatory cytokine-induced maturation of DCs, BMDCs were treated with CCNVs and recombinant TNF-α (100 ng/ml) and IFN-γ (20 ng/ml) (BioLegend)^{34,35}. Then, the BMDCs were detached and stained with the following antibodies: APC–Cy7 anti-mouse CD11c antibody, PE anti-mouse CD80 antibody and APC anti-mouse CD86 antibody (BioLegend). For TNF-α and IFN-γ knockdown, predesigned siRNA Silencer Select siRNA was purchased from Ambion Invitrogen, and siRNA transfection was conducted with Lipofectamine™ RNAiMAX Transfection Reagent (Thermo Fisher) according to the manufacturer’s protocol. Briefly, senescence was induced by doxorubicin treatment, and 24 h later, the B16F10 cells were washed with fresh medium, and siRNA was transfected on Day 1, 2, or 3 for optimization. After 3 days of culture, the cells were harvested, and the mRNA and protein levels of TNF-α and IFN-γ were tested by qRT–PCR and western blotting. Then, senescent B16F10 cells with TNF-α and IFN-γ knocked down were used to produce siRNA-transfected SCCNVs.

In vivo imaging of SCCNVs

For in vivo imaging of intradermally injected nanovesicles, CCNVs or SCCNVs were stained with VivoTrack 680 (Perkin Elmer, MA, USA) according to the manufacturer’s protocol. VivoTrack-stained CCNVs or SCCNVs (20 μg) were suspended in 50 μl of PBS and intradermally injected into the right flank of mice (*n* = 4 animals). To monitor the biodistribution of the injected SCCNVs, the mice were sacrificed 24 h after the injection. Five major organs (the heart, lungs, liver, kidneys and spleen) and the lymph nodes near the injection site were retrieved. Fluorescence signals were acquired using IVIS spectrum computed tomography (Perkin Elmer) at a 680-nm excitation wavelength and quantified using Living Image 3.1 software. The fluorescence intensity of each organ or lymph node was normalized to the sum of the intensities of the organs and tumors in each group.

In vivo DC maturation

For analysis of in vivo DC maturation, PBS, CCNVs or SCCNVs were intradermally injected into the right flank of 6-week-old C57BL/6 mice. Three days after the injection, the right inguinal lymph node was harvested from the mice, minced, and passed through a 70-μm pore filter. The separated single cells were stained with the following antibodies: PE-conjugated anti-mouse CD11c, APC-conjugated anti-mouse CD86 and FITC-conjugated anti-mouse MHC class I (BioLegend). Fluorescently labeled cells were analyzed with a BD Canto-II flow cytometer (BD Sciences). FACS data were analyzed using FlowJo software (TreeStar Inc.). To investigate DC accumulation in the lymph nodes after intradermal injection of PBS, CCNVs or SCCNVs, the right-side inguinal lymph nodes were harvested 7 days after the intradermal injection. Then, the lymph nodes were minced and passed through a 70-μm pore filter. The

separated single cells were stained with a PE-conjugated anti-mouse CD11c antibody, and the number of DCs was obtained through FACS analysis.

In vitro T-cell proliferation analysis

OVA-specific CD8⁺ T cells harvested from transgenic OT-1 mice were used for the in vitro T-cell proliferation assay. Briefly, the lymph nodes and spleen of OT-1 mice were harvested, minced, and passed through a 70- μ m pore filter. Then, CD8⁺ T cells were isolated using a MojoSort CD8⁺ T-cell isolation kit (BioLegend) according to the manufacturer's protocol. The isolated OT-1 CD8⁺ T cells were stained with a CFSE cell division tracker kit (BioLegend) and cocultured with splenocytes (including DCs) isolated from wild-type C57BL/6 mice. Then, 1 μ g/ml CCNVs and SCCNVs, which were produced from EL4 cancer cells or OVA-expressing E. G7-OVA cancer cells, was added to the cultures. An OVA epitope peptide (257-264, 1 mg/ml; ANASPEC, CA, USA) was used as the positive control. After 3 days of culture, the cells were harvested and stained with a BV421-conjugated anti-mouse CD3 antibody and PE-Cy7-conjugated anti-mouse CD8 antibody (BioLegend). Then, the percentage of CFSE^{low} CD3⁺ CD8⁺ T cells was calculated.

Mouse immunization model

To investigate the immune responses induced by SCCNVs, C57BL/6 mice were intradermally injected with PBS, CCNVs or SCCNVs three times every 6 days. Three days after injection, blood was harvested from the immunized mice through retro-orbital bleeding, and red blood cells and lymphocytes were collected by centrifugation at 3000 \times g for 30 min. Then, the red blood cells were lysed using RBC lysis buffer (Gibco). The lymphocytes were then stained with a BV421-conjugated anti-mouse CD3 antibody, an APC-conjugated anti-mouse CD4 antibody and a PE-Cy7-conjugated anti-mouse CD8 antibody (BioLegend) and analyzed with a BD Canto-II flow cytometer (BD Sciences). Six days after the last immunization, splenocytes were harvested from the mice and restimulated with 1 μ g/ml gp100 peptides, the antigenic epitope of B16F10 cancer cells, as described in previous studies²⁶. After 3 days of culture, the CD8⁺ T cells in the splenocytes were stained with a BV421-conjugated anti-mouse CD3 antibody, an APC-conjugated anti-mouse CD4 antibody and a PE-Cy7-conjugated anti-mouse CD8 antibody (BioLegend), and the culture supernatants were analyzed with IFN- γ and TNF- α ELISA kits (BioLegend). For CFSE staining, splenocytes were stained with CFSE first and then restimulated with gp100 peptides. After 3 days, the splenocytes were stained with an anti-mouse CD3 antibody and a PE-Cy7-conjugated anti-mouse CD8 antibody (BioLegend) and analyzed on a BD Canto-II to detect CFSE^{low} CD3⁺ CD8⁺ T cells. For ELISpot analysis, an ELISpot Plus: Mouse IFN- γ (ALP) (MabTech, Sweden) kit was used to analyze antigen-specific T cells in splenocytes. Harvested splenocytes were restimulated with gp100 peptides and cultured in ELISpot plates, and IFN- γ spots were counted after 24 h of culture.

In vivo prophylactic model

Six-week-old C57BL/6 mice were randomly divided into three groups, anesthetized with xylazine (10 mg/kg) and ketamine (100 mg/kg) and intradermally injected with PBS, CCNVs or SCCNVs (20 μ g of nanovesicles in 50 μ l of PBS) once a week for three weeks. Six days after the last immunization, the mice were subcutaneously injected with B16F10 cancer cells (5×10^5 cells in 100 μ l of PBS per mouse) in the right flank. Tumor size was measured every 3 days using a digital caliper and computed according to the ellipsoidal calculation formula: $V = 0.5 \times (\text{longest diameter}) \times (\text{shortest diameter})$. Mouse survival was monitored for 40 days. The mice bearing tumors exceeding 2,500 mm³ in size were euthanized with CO₂ inhalation.

In vivo tumor challenge model

Six-week-old C57BL/6 mice were anesthetized with rumpun (10 mg/kg) and ketamine (100 mg/kg) and subcutaneously injected with B16F10 cancer cells (5×10^5 cells in 100 μ l of PBS per mouse) in the right flank. On Days 5, 8, and 11, the mice were intradermally injected with PBS, CCNVs or SCCNVs (20 μ g of nanovesicles in 50 μ l of PBS). Tumor size was measured every 3 days using a digital caliper and computed according to the ellipsoidal calculation formula: $V = 0.5 \times (\text{longest diameter}) \times (\text{shortest diameter})$. Mouse survival was monitored for 30 days. The mice bearing tumors exceeding 2500 mm³ in size were euthanized with CO₂ inhalation.

Tumor-infiltrating lymphocyte analysis

Tumor-infiltrating lymphocytes were analyzed as previously described^{36,37}. Briefly, 4 days after the last injection, the tumor masses were harvested from euthanized mice and weighed. Then, the tumor tissues were minced and passed through a 70- μ m pore filter. The separated single cells were stained with the following antibodies: anti-mouse CD3, anti-mouse CD4, anti-mouse CD8, anti-mouse Foxp3, anti-mouse IFN- γ and anti-mouse TNF- α (BioLegend). Intracellular staining of tumor-infiltrating lymphocytes was conducted according to the manufacturer's protocol. The staining results were analyzed using FlowJo software (TreeStar Inc.).

Immunohistochemical staining of tumor sections

Tumor tissues were fixed in 4% PFA and kept in a 30% sucrose solution for 1 day. The fixed tissues were embedded in OCT (Scigen Scientific, CA, USA) and stored at -80 $^{\circ}$ C. The cryopreserved tissues were sectioned at a thickness of 10 μ m using a cryostat microtome (Leica, Germany). For Foxp3 staining, tissue sections were washed with PBS twice, blocked, and permeabilized with 0.6% Triton X-100 and 10% donkey serum (Gibco) in PBS for 2 h. Then, the sections were incubated with anti-mouse Foxp3 antibodies (BioLegend) overnight at 4 $^{\circ}$ C. Any unbound antibodies were removed, and the cell nuclei were stained with DAPI for 10 min. Fluorescence images were obtained with an LSM 710 confocal microscope (Carl Zeiss). For terminal deoxynucleotidyl transferase-mediated dUTP nick end labeling (TUNEL) staining assays, tumor tissue sections were washed and stained using the DeadEndTM Fluorometric TUNEL System (Promega, WI, USA) according to the manufacturer's protocol. Images were obtained with an LSM 710 (Carl Zeiss), and the TUNEL-positive cell percentage was calculated using NIH ImageJ software (Bethesda).

In vivo toxicity of SCCNVs

C57BL/6 mice were anesthetized with rumpun (10 mg/kg) and ketamine (100 mg/kg) and intradermally injected with PBS, CCNVs or SCCNVs (20 μ g of nanovesicles in 50 μ l of PBS). Blood samples were obtained at various time points. Serum was obtained from the blood samples by centrifugation at 3000 \times g for 30 min. The levels of AST, ALT, creatinine and BUN in the serum were determined with a DRI-CHEM 3500 S chemical analyzer (Fujifilm, Japan). For histological analysis, major organs (the liver, lungs, spleen, heart and kidneys) were harvested 14 days after the first injection. The tissues were fixed in 4% PFA overnight at 4 $^{\circ}$ C and dehydrated in a 30% sucrose solution. The tissues were embedded in OCT compound (Scigen Scientific) and sectioned at a thickness of 10 μ m using a cryostat microtome (Leica, Germany). The sections were stained with hematoxylin (Cancer Diagnostics, NC, USA) and eosin (BBC Biochemical, WA, USA) and imaged using an optical microscope (Olympus, Tokyo, Japan).

Lung metastasis tumor model

Six-week-old Balb/c mice were anesthetized with rumpun (10 mg/kg) and ketamine (100 mg/kg), and 5×10^4 4T1-Luc tumor cells were injected intravenously. On Days 1, 4, and 7, PBS or 4T1-Luc cancer

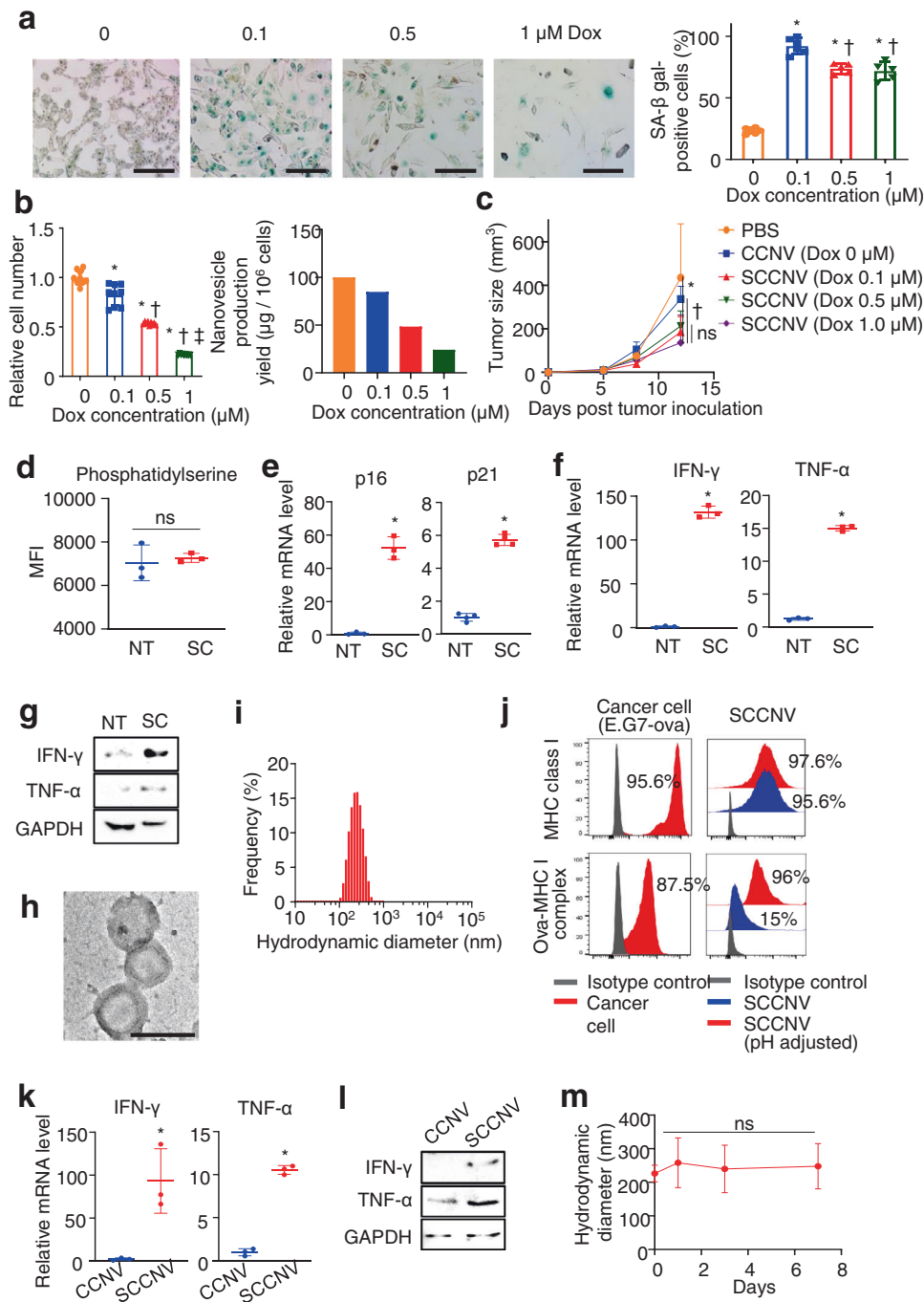


Fig. 2 **Characterization of SCCNVs.** **a** SA β -gal staining (green) of B16F10 cancer cells following senescence induction by treatment with various concentrations of doxorubicin for 4 days. Scale bars = 100 μm . **b** Optimization of the Dox concentration: the cell number relative to the initial cell number and nanovesicle production yield of B16F10 cancer cells after doxorubicin treatment at various concentrations for 4 days. **c** Optimization of the Dox concentration: antitumor efficacy of SCCNVs produced from cancer cells treated with various doxorubicin concentrations. $n = 3-5$. **d** Phosphatidylserine exposure on the B16F10 cancer cell surface after senescence induction with 0.1 μM doxorubicin, as evaluated by flow cytometric analysis. NT no treatment, SC senescence induction. $n = 3$. mRNA levels of **(e)** p16 and p21, **(f)** IFN- γ and TNF- α and **(g)** protein levels of IFN- γ and TNF- α in B16F10 cancer cells after senescence induction with 0.1 μM doxorubicin. NT no treatment, SC senescence induction. **h** Transmission electron microscopy image of SCCNVs. Scale bar = 250 nm. **i** Hydrodynamic diameter of SCCNVs. **j** Detection of the ovalbumin epitope presented on MHC class I expressed by E.G7-OVA cancer cells by FACS analysis. Following extrusion through nanosized pores, 15% of SCCNVs were positive for the OVA-MHC I complex. pH adjustment enabled the detached OVA in the supernatant to be reloaded on MHC I molecules, increasing the proportion of OVA-MHC I-positive SCCNVs to 96%. Relative **(k)** mRNA and **(l)** protein levels of IFN- γ and TNF- α in CCNVs and SCCNVs. **m** Hydrodynamic diameter of SCCNVs incubated in 10% (v/v) serum-containing buffer for various time periods, showing the colloidal stability of the SCCNVs. ns not significant. Data represent the mean \pm SD. Statistical significance was calculated by Student's t -tests (**e**, **f**, and **k**) or one-way analysis of variance (ANOVA) with Tukey's multiple comparisons test (**a**, **b**, and **m**). * $P < 0.05$ versus NT or 0 μM doxorubicin in (**a-f**), versus CCNVs in **i**. † $P < 0.05$ versus 0.1 μM in **a** and **b**, † $P < 0.05$ versus 0.5 μM in **b**.

cell-derived CCNVs or SCCNVs were intradermally injected. On Days 3, 6, and 9, 200 µg of anti-programmed death-ligand 1 (PD-L1) antibodies (BioXCell, NH, USA) was intraperitoneally injected to evaluate the synergistic antitumor efficacy with SCCNVs. To obtain bioluminescence images, prior to imaging, D-luciferin potassium salt (Gold Biotechnology, MO, USA) in sterile water was injected intraperitoneally according to the manufacturer's protocol³³. Bioluminescence images were acquired by IVIS spectrum computed tomography (Perkin Elmer), and the total luminescence flux in lung tissues was quantified using Living Image 3.1 software. On Day 15, a 15% India ink solution was injected intratracheally, and the India ink-stained lung tissues were harvested. The harvested lung tissues were washed with distilled water and fixed in Fekete's solution overnight. Then, images of the India ink-stained lung tissues were obtained, with tumor nodules visualized in white.

Postsurgery tumor model

Six-week-old C57BL/6 mice were anesthetized with rumpun (10 mg/kg) and ketamine (100 mg/kg) and subcutaneously injected with B16F10 cancer cells (5×10^5 cells in 100 µL PBS per mouse) in the right flank. On Day 14, when the tumor volume reached $\sim 500 \text{ mm}^3$, the mice were anesthetized with rumpun and ketamine, and the tumor tissues were excised. On Day 17, the mice were randomly divided into three groups, and they were intradermally injected with PBS, CCNVs or SCCNVs (20 µg of nanovesicles in 50 µL of PBS) on Day 17 and Day 23. Tumor size was measured every 2 days using a digital caliper and computed according to the ellipsoidal calculation formula: $V = 0.5 \times (\text{longest diameter}) \times (\text{shortest diameter})$. Mouse survival was monitored for 35 days. The mice bearing tumors exceeding $2,500 \text{ mm}^3$ in size were euthanized with CO₂ inhalation. For immunohistochemical staining of tumor tissues, tumor tissues were harvested on Day 27. The tumor tissues were analyzed with the DeadEnd™ Fluorometric TUNEL System (Promega, WI, USA) according to the manufacturer's protocol. For the postsurgery 4T1 breast cancer model, 5×10^5 cells in 100 µL of PBS per mouse were inoculated into the right flank. When the tumor size reached $\sim 200 \text{ mm}^3$, the tumor tissues were excised, and PBS or 4T1 cancer cell-derived CCNVs or SCCNVs were injected. Tumor size was measured every 3 days.

Statistical analysis

Unless described otherwise, data are presented as the mean \pm standard deviation (SD). Data were analyzed through one-way analysis of variance (ANOVA) with Tukey's multiple comparisons test to calculate *P*-values for comparisons among more than two groups. Two-way ANOVA with Bonferroni's correction or Holm–Sidak posttests was used to calculate the *P*-values for comparisons among groups over multiple time points. The log-rank test was used to compare survival differences shown in Kaplan–Meier plots using Prism software (GraphPad, CA, USA).

RESULTS

To induce senescence in B16F10 melanoma cells, cells were treated with various concentrations of doxorubicin. Senescence-associated beta-galactosidase (SA-β-gal) staining showed that doxorubicin concentrations higher than 0.1 µM successfully induced senescence. A doxorubicin concentration of 0.1 µM resulted in the highest cell viability and nanovesicle production yield (Fig. 2a, b). The *in vivo* antitumor efficacy of SCCNVs was not significantly different across the 0.1–1.0 µM range of doxorubicin concentrations used for SCCNV preparation (Fig. 2c). Thus, we chose 0.1 µM as the optimal concentration of doxorubicin and used this concentration in subsequent experiments. This concentration was 100 times lower than that used for clinical chemotherapy, and the residual doxorubicin after doxorubicin treatment of cells was removed prior to the use of SCCNVs in experiments. Therefore, doxorubicin itself would not exert unexpected antitumor effects in

SCCNV therapy. Exposure of phosphatidylserine on the B16F10 cell surface did not show a significant change before and after 0.1 µM doxorubicin treatment (Fig. 2d), indicating that 0.1 µM doxorubicin treatment did not induce severe apoptosis of B16F10 cells. The mRNA expression levels of p16 and p21, cellular senescence markers, were increased in B16F10 cells treated with 0.1 µM doxorubicin (Fig. 2e). In addition, the mRNA and protein levels of IFN-γ and TNF-α, both of which are SASP markers induced in senescent cells, were increased in B16F10 cells treated with 0.1 µM doxorubicin (Fig. 2f, g). Transmission electron microscopy (TEM) analysis showed a unilamellar structure with lipid bilayers of SCCNVs (Fig. 2h; Supplementary Fig. 1). SCCNVs showed hydrodynamic diameters of $226.1 \pm 24.6 \text{ nm}$, as revealed by dynamic light scattering analysis (Fig. 2i), and the zeta potential of SCCNVs was -20.2 ± 8.7 (Supplementary Fig. 2). Coomassie blue staining revealed that senescence induction did not change the protein profiles of B16F10 cancer cells, and SCCNVs preserved most of the proteins from senescent B16F10 cancer cells, with a small variation possibly due to the relative increase in cell-surface proteins through nanovesicle production (Supplementary Fig. 3)²³. Next, we investigated whether the antigens presented by MHC class I on cancer cells were preserved on SCCNVs by FACS analysis (Fig. 2j). SCCNVs were produced from E.G7-OVA cancer cells, which present the ovalbumin (OVA) epitope (SIINFEKL) on MHC class I molecules. Extrusion through nanosized pores induced antigen detachment from MHC class I and reduced the portion of OVA–MHC class I complex-positive SCCNVs to 15%. Following extrusion, adjustment of the pH in the SCCNV-containing solution to 5.5 for 30 min^{31,32} induced complete reloading of the antigens on MHC class I. There was no significant difference in antitumor efficacy between SCCNVs and pH-adjusted SCCNVs, indicating that the partial loss of antigens presented on MHC class I did not affect the antitumor efficacy of SCCNVs (Supplementary Fig. 4). The increased IFN-γ and TNF-α levels in senescence-induced cells were preserved in SCCNVs at both the mRNA and protein levels (Fig. 2k, l). The amounts of IFN-γ and TNF-α in SCCNVs were quantified by enzyme-linked immunosorbent assay (ELISA), and approximately 4.56 pg of IFN-γ and 0.14 pg of TNF-α were included in 1 µg of SCCNVs (Supplementary Fig. 5). Finally, the hydrodynamic diameter of SCCNVs was monitored for one week, and the results showed that the size of SCCNVs was stably maintained in serum-containing buffer for at least 7 days (Fig. 2m).

Next, we investigated whether SCCNVs can promote DC maturation *in vitro*. DCs can internalize both SCCNVs and cancer cell-derived nanovesicles (CCNVs), and the uptake efficiency was not different between SCCNVs and CCNVs (Fig. 3a). SCCNV-treated DCs showed significantly higher mRNA levels of IL-6 and IL-12p40 (DC maturation markers) than CCNV-treated DCs, indicating that the SCCNVs stimulated DC maturation (Fig. 3b). CCNVs did not stimulate sufficient DC maturation since there were no differences in the mRNA levels of IL-6 and IL-12p40 between the PBS and CCNV groups. FACS analysis of CD86, CD80 and MHC class I expressed on DCs confirmed the stimulation of DC maturation by SCCNVs (Fig. 3c, d). FACS analysis revealed that TNF-α and IFN-γ significantly enhanced DC maturation, as shown comparing the CCNV group and the CCNV + TNF-α + IFN-γ group (Fig. 3e). In addition, siRNA-SCCNVs were produced from B16F10 cancer cells that were treated with doxorubicin and transfected with siRNAs specific for IFN-γ and TNF-α. siRNA transfection induced knock-down of IFN-γ and TNF-α in doxorubicin-treated B16F10 cancer cells (Supplementary Fig. 6). siRNA-SCCNVs were less effective in inducing DC maturation than SCCNVs (Fig. 3f). These data indicate that the enhanced DC maturation induced by SCCNV treatment is due to IFN-γ and TNF-α contained in the SCCNVs. This suggests that a significant portion of the stimulatory effect of SCCNVs on DC maturation is due to TNF-α and IFN-γ delivered by the SCCNVs.

Ex vivo imaging performed 24 h after intradermal injection of fluorescently labeled SCCNVs or CCNVs showed that SCCNV

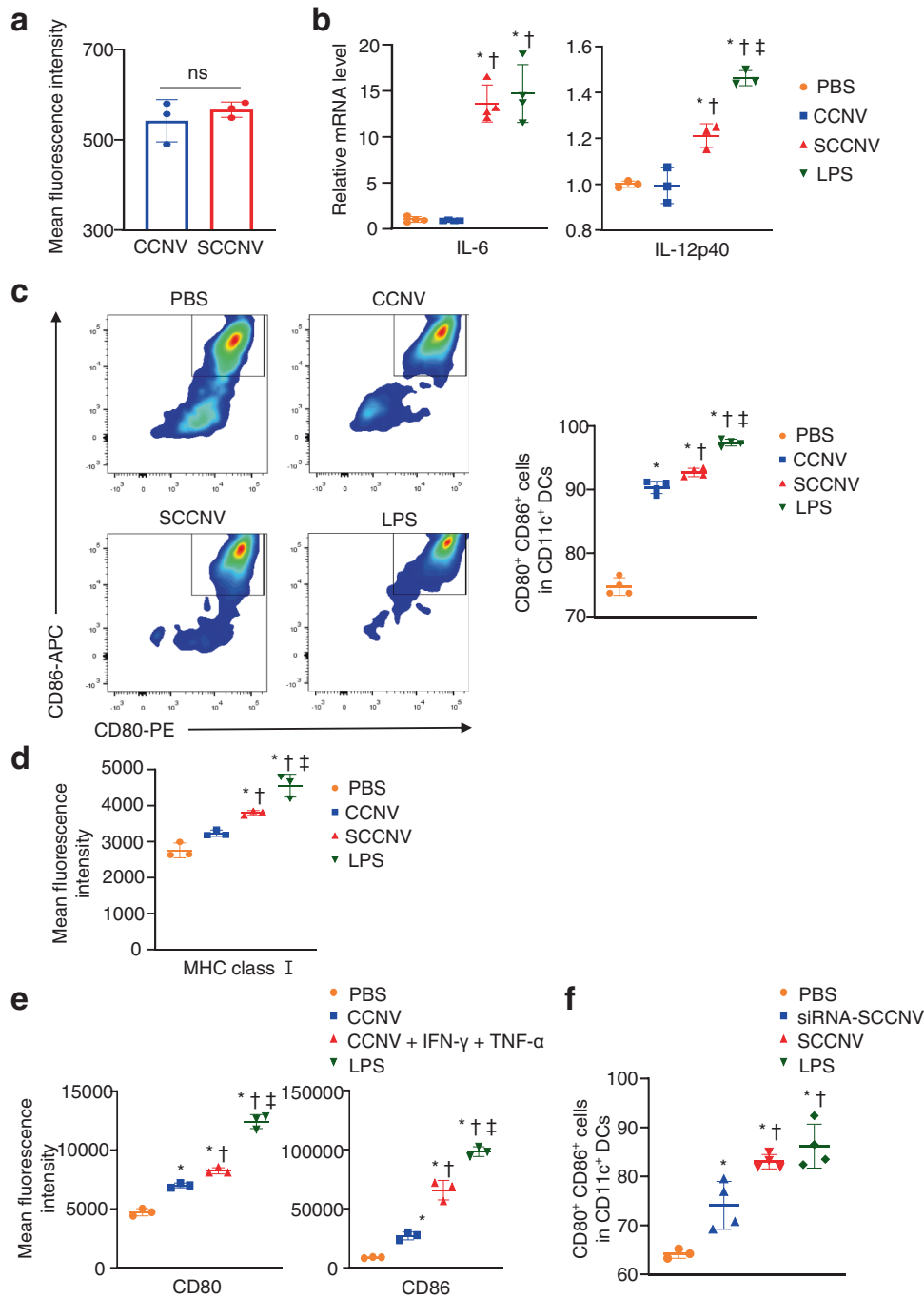


Fig. 3 Effective DC maturation in vitro by SCCNVs. **a** In vitro uptake of CCNVs and SCCNVs by DCs for 10 min, as evaluated by flow cytometric analysis. $n = 3$. **b** mRNA levels of DC maturation markers (IL-6 and IL-12p40) in BMDCs treated with PBS, CCNV, SCCNV, or LPS for 4 h in vitro, as evaluated by qRT-PCR. $n = 3$ –4. **c** Representative flow cytometry plot and percentage of CD80 and CD86 double-positive cells in BMDCs treated with PBS, CCNV, SCCNV, or LPS for 24 h in vitro, evaluated by flow cytometric analysis. $n = 4$. **d** Flow cytometric analysis of MHC class I expression of BMDCs treated with PBS, CCNVs, SCCNVs, or LPS for 24 h in vitro, as evaluated by flow cytometric analysis. $n = 3$. **e** Flow cytometric analysis showing that the enhanced DC maturation induced by SCCNVs is likely due to IFN- γ and TNF- α contained in SCCNVs. Exogenous IFN- γ and TNF- α were added to the CCNV + IFN- γ + TNF- α group. $n = 4$. **f** Effects of various treatments for 24 h on DC maturation, as evaluated by flow cytometric analysis. siRNA-SCCNVs are nanovesicles derived from senescent cancer cells transfected with siRNA specific for IFN- γ and TNF- α . $n = 4$. In (**b**–**f**), LPS was used as the positive control. Data represent the mean \pm SD. Statistical significance was calculated by Student's *t*-tests or one-way ANOVA with Tukey's multiple comparisons test. * $P < 0.05$ versus PBS; † $P < 0.05$ versus CCNVs; ‡ $P < 0.05$ versus SCCNVs in **b**, **c**, **d** and **f** and versus CCNVs + IFN- γ , TNF- α in **e**. ns not significant.

migration to the draining lymph nodes was significantly higher than that of CCNVs (Fig. 4a). Several studies have shown that nanoparticles larger than 100 nm migrate into the lymph nodes by cellular uptake^{38–40}. Therefore, this result may be attributed to the fact that SCCNV uptake by immature DCs stimulates DC

maturation, leading to the subsequent migration of mature DCs to the draining lymph nodes, while CCNV uptake does not stimulate DC maturation. To investigate the in vivo maturation of DCs, DCs in the draining lymph nodes were analyzed 3 days after intradermal injection of SCCNVs. DCs harvested from SCCNV-

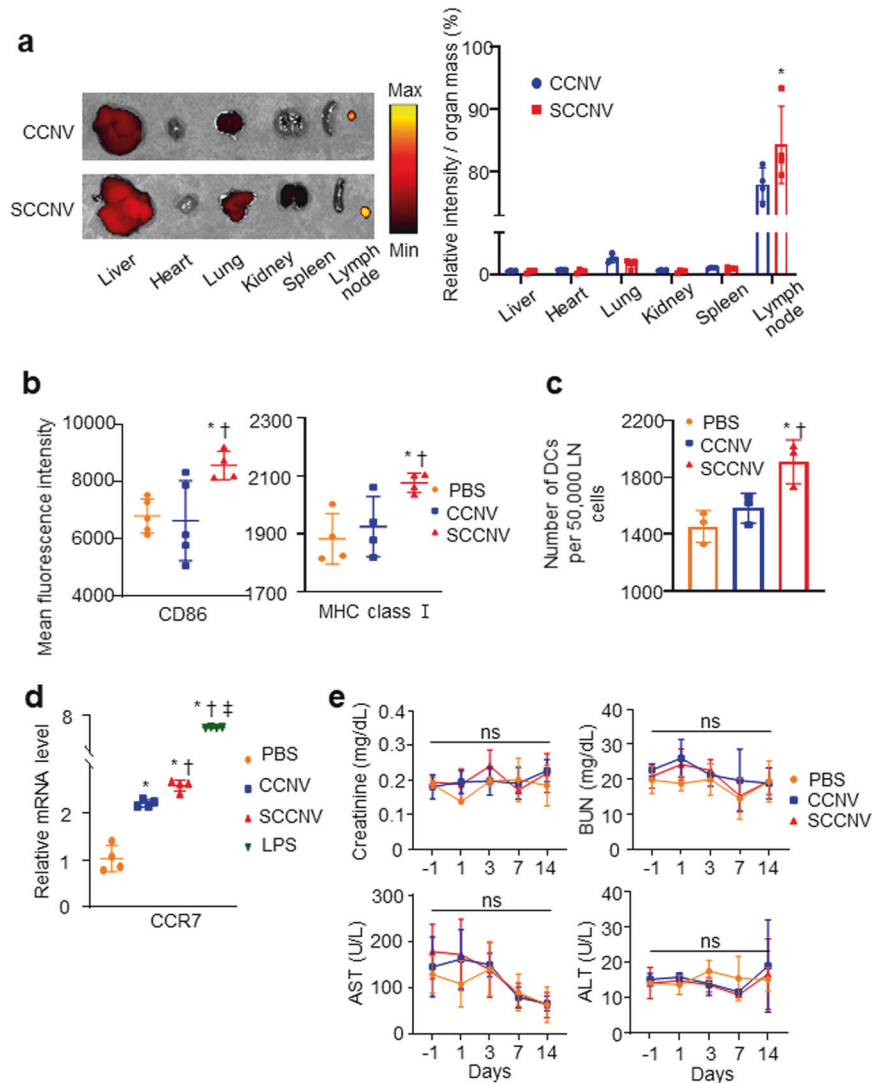


Fig. 4 Effective homing of SCCNVs to lymph nodes, DC maturation in vivo, and SCCNV toxicity. **a** Ex vivo imaging at 24 h after intradermal injection of fluorescently labeled CCNVs and SCCNVs. Relative fluorescence was divided by organ mass. *n* = 4. **b** Maturation marker expression in dendritic cells in the draining lymph nodes 3 days after intradermal injection of PBS, CCNVs, or SCCNVs, as evaluated by flow cytometric analysis. *n* = 4–5. **c** Number of dendritic cells in the draining lymph nodes 7 days after intradermal injection of PBS, CCNVs, or SCCNVs, as evaluated by flow cytometric analysis. *n* = 3. **d** mRNA level of CCR7, a representative marker of DC migration to secondary lymphoid organs, in BMDCs treated with PBS, CCNV, SCCNV, or LPS for 24 h in vitro. *n* = 4. **e** Serum levels of creatinine, BUN, AST, and ALT in mice treated with intradermal injection of PBS, CCNVs, or SCCNVs three times. *n* = 4. Statistical significance was calculated by one-way analysis of variance (ANOVA) with Tukey's multiple comparisons test or two-way analysis of variance with Bonferroni posttests. **P* < 0.05 versus CCNVs in **a** and versus PBS in **(b–d)**; †*P* < 0.05 versus CCNVs in **(b–d)**; ‡*P* < 0.05 versus SCCNVs in **d**. ns not significant.

injected mice showed relatively high expression of CD86 and MHC class I (Fig. 4b), revealing that SCCNVs facilitated DC maturation in vivo. Seven days after intradermal injection, the DC population in the draining lymph nodes was significantly larger in the SCCNV injection group than in the CCNV or PBS injection group (Fig. 4c). The mRNA level of CCR7, a marker related to DC migration to secondary lymphoid organs, was significantly increased in the SCCNV injection group compared to the CCNV or PBS injection group (Fig. 4d). Injected SCCNVs did not induce toxicity in the liver, kidneys or other major organs (Fig. 4e; Supplementary Fig. 7).

Given that SCCNVs stimulated DC maturation in vivo, we next investigated whether SCCNVs could promote the activation of tumor-specific T cells. Carboxyfluorescein succinimidyl ester (CFSE)-labeled OT-1 CD8⁺ T cells were cocultured with splenic DCs that had been pulsed with PBS, OVA peptide, CCNVs or SCCNVs. The CCNVs and SCCNVs were derived from EL4-cancer cells or E.G7-OVA cancer cells. The group containing SCCNV-

pulsed DCs showed significantly higher activation of OVA-specific T cells (OT-1 transgenic mouse-derived cells) than the other groups, as shown by the lower mean fluorescence intensity of CFSE-stained CD8⁺ T cells in the SCCNV group (Fig. 5a). The positive control (the OVA peptide group) confirmed that T-cell proliferation was due to OVA presented by DCs. To investigate whether SCCNVs promote T-cell activation in vivo, B16F10 cancer cell-derived SCCNVs, B16F10 cancer cell-derived CCNVs, or PBS was injected intradermally into mice, and peripheral blood mononuclear cells (PBMCs) and splenocytes were collected and analyzed (Fig. 5b). After immunization, the population of CD8⁺ T cells in PBMCs was significantly increased in the SCCNV injection group (Fig. 5c). Splenocytes isolated from immunized mice were restimulated in vitro with gp100 peptides (tumor antigen of B16F10 cancer cells) or PMA/ionomycin as a positive control. The SCCNV injection group showed a higher ratio of CD8⁺ T cells/CD3⁺ T cells and stronger proliferation of CD8⁺ T cells (Fig. 5d, e).

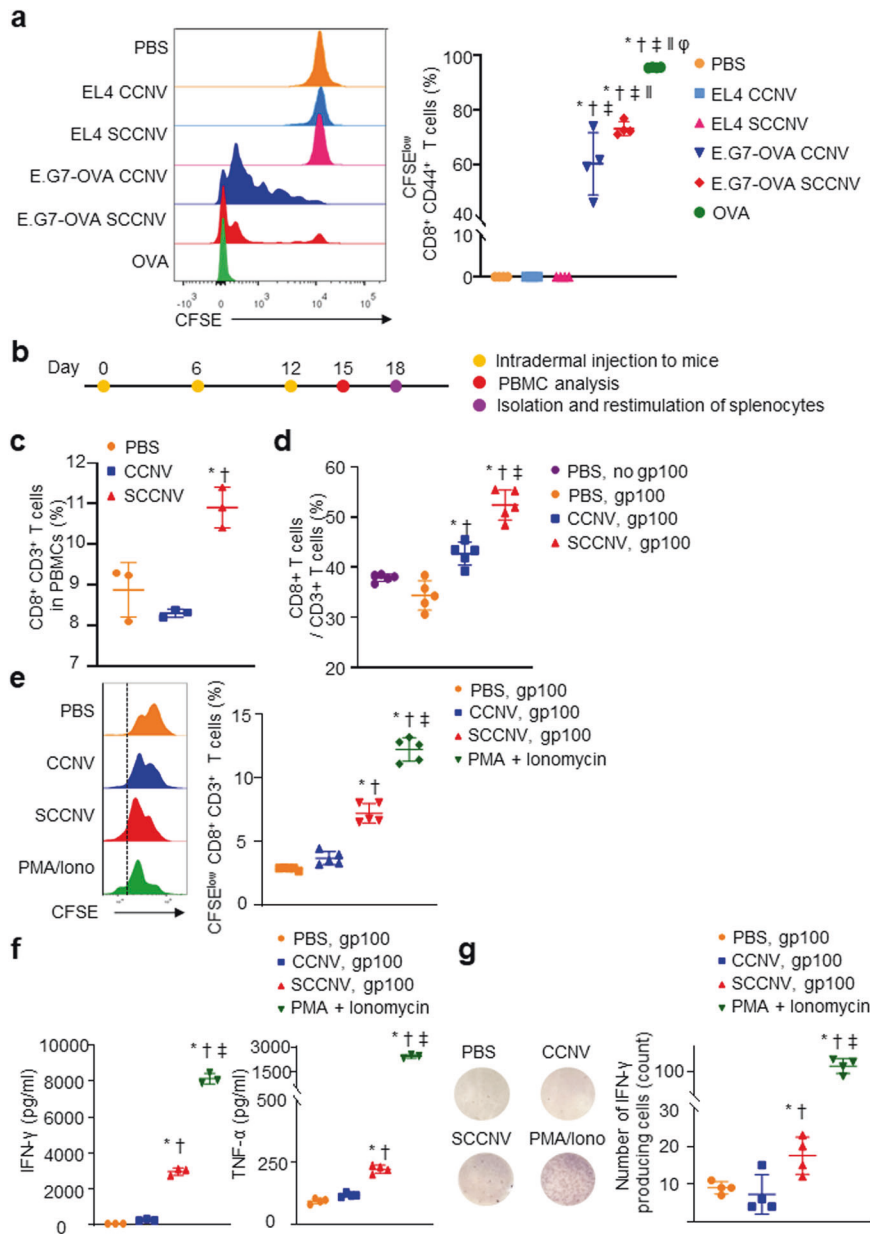


Fig. 5 Effective activation of tumor-specific CD8⁺ T cells by SCCNVs in vitro and in vivo. **a** Flow cytometric analysis of the in vitro proliferation of naïve OT-I CD8⁺ T cells labeled with CFSE and subsequently cocultured for 72 h with splenic DCs that had been pulsed with PBS, ovalbumin peptide (OVA), CCNVs or SCCNVs. CCNVs and SCCNVs were produced from EL4-cancer cells or E.G7-OVA cancer cells. OVA was used as the positive control. **b** Timeline for the C57BL/6 mouse immunization study. **c** Flow cytometric analysis of CD8⁺ T cells in the PBMCs of mice immunized with intradermal injection of PBS, B16F10 cancer cell-derived CCNVs, or SCCNVs. **d** Ratio of CD8⁺/CD3⁺ T cells in splenocytes harvested from mice that were immunized with PBS, B16F10 cancer cell-derived CCNVs, or SCCNVs and subsequently restimulated in vitro with the gp100 peptide (the tumor antigen of B16F10 cancer cells) for 72 h. **e** In vitro proliferation of CD8⁺ T cells during the restimulation of CFSE-labeled splenocytes harvested from mice that had been immunized with PBS, B16F10 cancer cell-derived CCNVs, or SCCNVs. PMA/ionomycin (T-cell activation-inducing agents) served as the positive control. **f** Levels of IFN- γ and TNF- α , both of which are CD8⁺ T-cell activation markers, in the culture medium following the in vitro restimulation of splenocytes. The levels of IFN- γ and TNF- α were evaluated with ELISA. **g** ELISpot analysis of splenocytes harvested from mice immunized with various agents. The number of IFN- γ -producing cells per well was evaluated ($n = 4$). Statistical significance was calculated by one-way ANOVA with Tukey's multiple comparisons test. * $P < 0.05$ versus PBS in (a–c) and (e–g) or versus PBS, no gp100 in d; † $P < 0.05$ versus EL4 cancer cell-derived CCNVs in a, versus CCNV in c, e, f and g, and versus PBS, gp100 in d; ‡ $P < 0.05$ versus EL4 cancer cell-derived SCCNVs in (a), versus CCNVs in (d), and versus SCCNV in e, f and g; || $P < 0.05$ versus CCNVs in a; $\phi P < 0.05$ versus SCCNVs in a.

Enzyme-linked immunosorbent assay (ELISA) analysis of supernatants from cultures of gp100-pulsed splenocytes isolated from various groups of mice revealed higher IFN- γ and TNF- α levels in SCCNV-immunized mice (Fig. 5f), and an enzyme-linked immunosorbent assay (ELISpot) showed a higher number of IFN- γ -producing gp100-specific T cells in the spleen of SCCNV-immunized mice

than in that of CCNV-immunized mice (Fig. 5g). Together, these results indicated that SCCNV immunization more effectively stimulated the activation of vaccine antigen (gp100)-specific CD8⁺ T cells than did CCNV immunization.

Next, we investigated whether SCCNVs can suppress tumor growth in therapeutic and prophylactic melanoma mouse models.

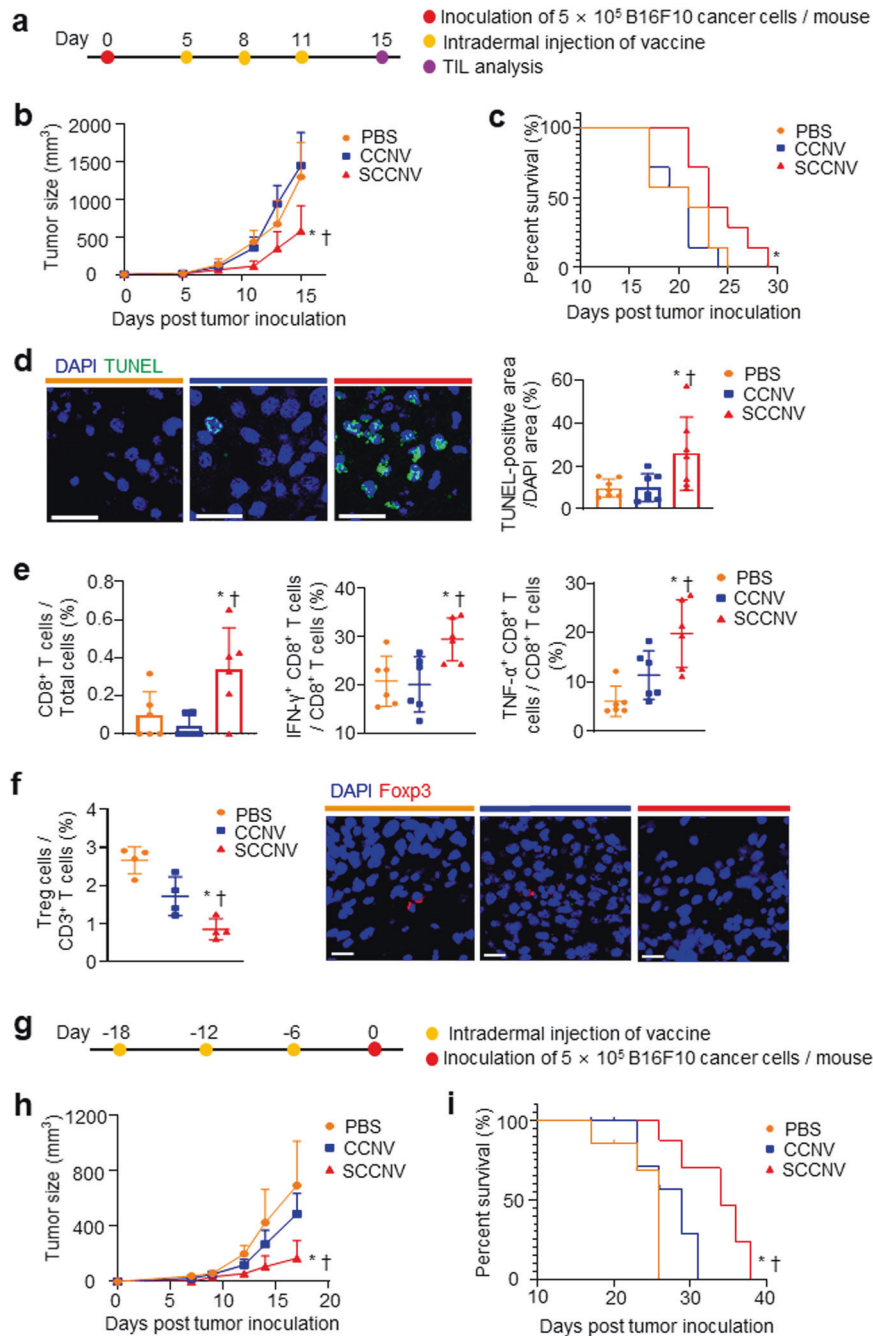


Fig. 6 Therapeutic efficacy of SCCNVs in a therapeutic melanoma murine model and a prophylactic melanoma murine model. **a** Therapeutic tumor modeling and vaccination timeline for (b–f). **b** Tumor growth profile. $n = 6$. **c** Animal survival rate. $n = 6$. **d** TUNEL staining of tumor tissues harvested on Day 15. $n = 7$. Scale bars = 100 μm . **e** Immunohistochemical staining for CD8 + T cells in tumor tissues and flow cytometric TIL analysis of tumor tissues harvested on Day 15. $n = 6$. **f** Percentage of Treg cells measured in the flow cytometric TIL analysis ($n = 4$) and immunohistochemical staining for Foxp3 in tumor tissues harvested on Day 15. Scale bars = 50 μm . **g** Vaccination and prophylactic tumor modeling timeline for (h) and (i). **h** Tumor growth profile. $n = 5$. **i** Animal survival rate. $n = 5$. Statistical significance was calculated by the log-rank (Mantel–Cox) test (c and i), one-way ANOVA with Tukey’s multiple comparisons test (d–f) or by two-way ANOVA with Bonferroni posttests (b and h). * $P < 0.05$ versus PBS; † $P < 0.05$ versus CCNVs.

SCCNVs were injected intradermally into B16F10 tumor-bearing mice (Fig. 6a). SCCNVs significantly suppressed tumor growth in vivo and improved animal survival (Fig. 6b, c; Supplementary Fig. 8). A terminal deoxynucleotidyl transferase dUTP nick end labeling (TUNEL) staining assay showed a significantly higher density of apoptotic cells in tumor tissues in the SCCNV-immunized group (Fig. 6d). Immunohistochemical (IHC) staining and tumor-infiltrating lymphocyte (TIL) analysis of tumor tissues

showed significantly higher densities of activated (IFN- γ - or TNF- α -positive) cytotoxic T cells in the SCCNV-immunized group (Fig. 6e; Supplementary Fig. 9 and 10). Moreover, TIL analysis and IHC staining showed that the regulatory T-cell density was significantly lower in the SCCNV-immunized group, indicating a proinflammatory microenvironment in the SCCNV-immunized group (Fig. 6f). Furthermore, in the prophylactic model, mice that underwent immunization were challenged with B16F10 melanoma cells (Fig.

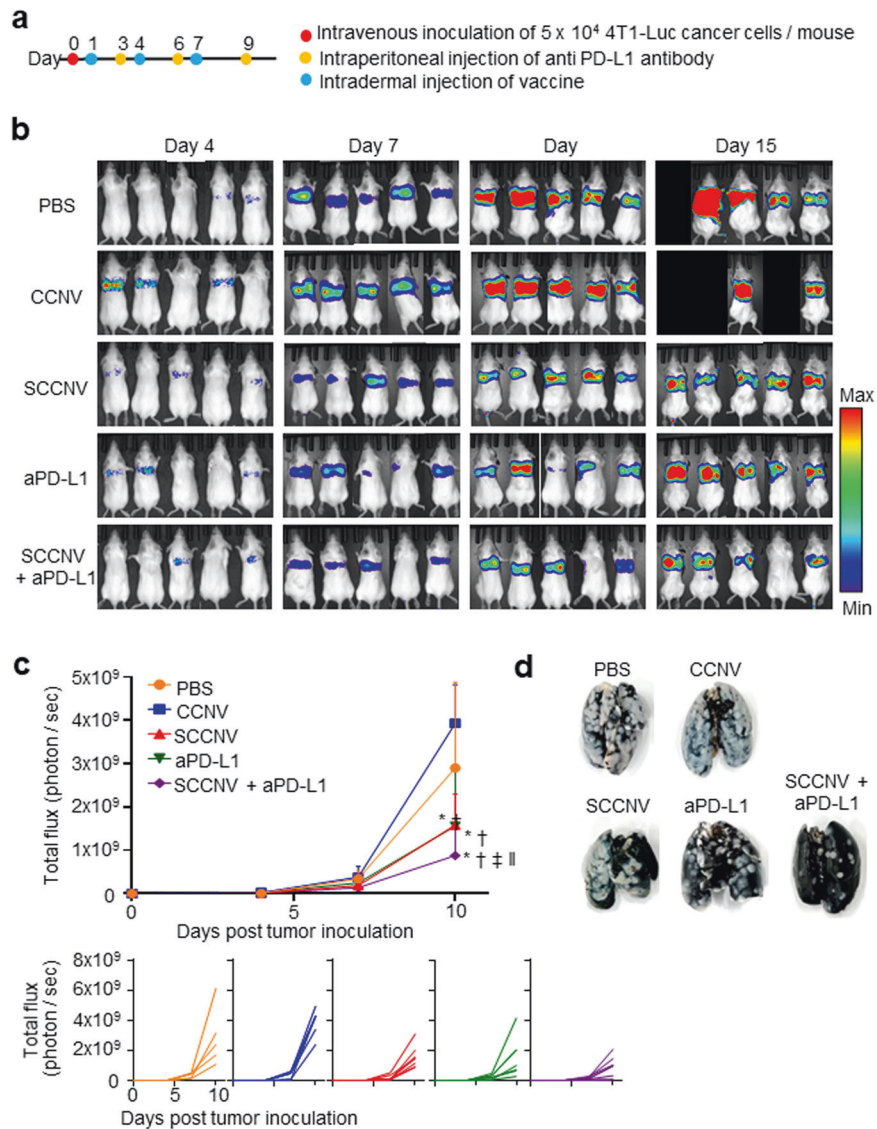


Fig. 7 Inhibition of tumor metastasis by SCCNV injection in murine models. **a** Timeline for metastasis modeling of 4T1-Luc tumors with vaccination. **b** Representative bioluminescence images and **c** luminescence flux showing tumor metastasis to the lungs in 4T1-Luc tumor cell-inoculated mice at various time points. $n = 5-6$. **d** Images of lungs harvested on Day 15 and stained with India ink. Tumor nodules were stained white, and normal lung tissues were stained black. Statistical significance was calculated by two-way ANOVA with Holm-Sidak posttests. * $P < 0.05$ versus PBS; † $P < 0.05$ versus CCNVs; ‡ $P < 0.05$ versus SCCNVs; || $P < 0.05$ versus aPD-L1.

6g). SCCNV immunization inhibited tumor growth more effectively and resulted in a significantly higher survival rate than CCNV or PBS immunization (Fig. 6h, i; Supplementary Fig. 11).

Next, we investigated whether SCCNV injection could suppress the metastatic growth of 4T1-Luc breast cancer cells, and anti-programmed death-ligand 1 (PD-L1) antibodies were administered to assess combination therapy (Fig. 7a). PD-L1 expression on 4T1-Luc cancer cells was confirmed by FACS analysis (Supplementary Fig. 12). Live bioluminescence imaging of metastatic tumor-bearing mice revealed that SCCNV vaccination significantly suppressed lung metastasis (Fig. 7b, c). Lung metastasis visualization with India ink staining confirmed the live bioluminescence imaging results (Fig. 7d). Importantly, SCCNV monotherapy produced a therapeutic outcome similar to that achieved with anti-programmed death-ligand 1 (PD-L1) antibody therapy at a clinical dose in this metastatic model. SCCNV vaccination successfully synergized with the anti-PD-L1 antibody, which prevented inactivation of tumor-reactive T cells in the immunosuppressive tumor microenvironment (Fig. 7b-d).

Finally, we investigated whether SCCNV vaccination could inhibit tumor recurrence in postsurgery models of B16F10 melanoma and 4T1-Luc breast cancer. When the melanoma tumor volume reached $\sim 500 \text{ mm}^3$, the tumor tissues were removed, and the mice were vaccinated with B16F10 cell-derived SCCNVs (Fig. 8a). SCCNV vaccination inhibited tumor recurrence more effectively (Fig. 8b; Supplementary Fig. 13) and produced significantly higher survival rates (Fig. 8c) than PBS or CCNV injection. A TUNEL staining assay showed that SCCNV injection resulted in a significantly higher density of apoptotic cells in tumor tissues (Fig. 8d). Additionally, in the 4T1-Luc breast cancer model, SCCNV vaccination inhibited tumor recurrence more effectively than PBS or CCNV injection (Fig. 8e, f).

DISCUSSION

As exosomes secreted by cancer cells in the TME may stimulate tumor growth by mediating crosstalk between cancer cells and immune cells in the TME⁴¹, and SCCNVs may be similar to cancer

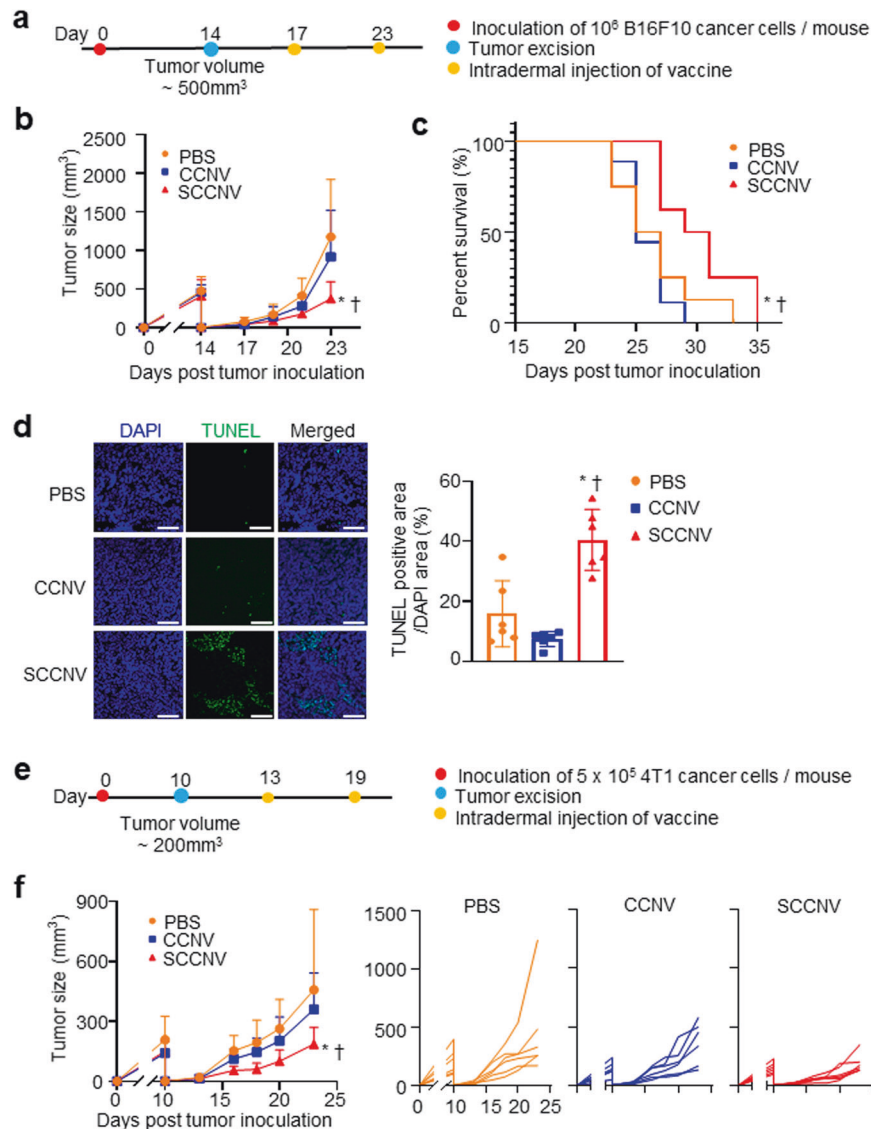


Fig. 8 Inhibition of postsurgery recurrence of melanoma and 4T1 tumors by SCCNV injection in murine models. **a** Timeline of postsurgery recurrence in the B16F10 tumor model for **(b–d)**. **b** Tumor growth profile. $n = 13$. **c** Animal survival rate. $n = 8$. **d** TUNEL staining of tumor tissues harvested on Day 27. $n = 6$. Scale bars = $100\ \mu\text{m}$. **e** Timeline of postsurgery recurrence in the 4T1 tumor model. **f** Tumor growth profile. $n = 6$. Statistical significance was calculated by two-way ANOVA with Bonferroni posttests (**b** and **f**), the log-rank (Mantel–Cox) test (**c**), or one-way ANOVA with Tukey’s multiple comparisons test (**d**). * $P < 0.05$ versus PBS; † $P < 0.05$ versus CCNVs.

cell-derived exosomes⁴². However, SCCNVs did not stimulate tumor growth because SCCNVs were injected intradermally and internalized by DCs in a tumor-free region, which prevents crosstalk between SCCNVs and immune cells in the TME.

Tumor lysates, which may have a similar composition to cancer cell-derived nanovesicles, can also be used as a potential TCV to deliver tumor antigens. However, tumor lysate vaccination generally results in low-efficiency DC activation and, in turn, weak antitumor immunity⁴³. In contrast, SCCNVs can deliver tumor antigens and proinflammatory cytokines (IFN- γ and TNF- α) simultaneously to DCs, leading to a higher efficiency of DC activation. Effective DC activation led to effective activation of tumor antigen-specific T cells and tumor inhibition in various mouse tumor models, including a prophylactic model, primary tumor model, metastasis model and postsurgery tumor recurrence model. These results show the potential of SCCNVs as a TCV.

SCCNVs may be clinically feasible for development into a personalized TCV. In the present study, we treated tumor-bearing model mice with SCCNVs derived from *in vitro* senescence-

induced cancer cell lines because most of the antigens of these immortalized cell lines are preserved over a short period⁴⁴. The heterogeneity of tumor cells and the difficulty of neoantigen identification make tumor treatment difficult. However, SCCNVs obtained from autologous tumor tissues would provide a patient-specific spectrum of tumor antigens with no need for neoantigen identification. Therefore, SCCNVs may be applied in the context of liquid tumors, such as acute myeloid leukemia, which have a small chance of being treated with immunotherapy due to the limited identification of tumor antigens and low response rate for immune checkpoint blockade^{45,46}. For solid tumors, SCCNVs, as personalized TCVs, could be prepared from autologous tumor tissues removed during surgery in end-stage cancer patients in whom surgical removal of tumor tissues may be necessary. In addition, SCCNVs could be used to eliminate metastatic cancer cells and prevent tumor recurrence in end-stage cancer patients, in whom metastasis or tumor recurrence is often observed.

Currently, several ongoing clinical trials are evaluating the efficacy of TCVs with neoantigens in the form of peptides

(NCT03639714, NCT03223103 and NCT02721043), mRNA (NCT04163094) or DNA (NCT04015700 and NCT04251117). However, the development of TCVs employing neoantigens is limited by the difficulty and labor intensiveness of this approach, as well as patient-to-patient variations in neoantigens. Only a small fraction (~1–2%) of mutations in cancer cells induce antitumor immune responses¹⁵, and only a small number of neoantigens are shared among cancer patients¹⁰. TCV therapy employing a single neoantigen may fail for tumors that undergo constant mutation and consequently evade recognition by vaccine-activated T cells⁴⁷. In contrast, SCCNVs produced from autologous cancer cells can avoid the labor-intensive and time-consuming processes needed for the identification of immunogenic neoantigens in individual patients and be free from the concern of patient-to-patient variations.

In conclusion, this study suggests the use of SCCNVs as a potential personalized TCV strategy. SCCNVs prepared from autologous (possibly heterogeneous) cancer cells can deliver a broad spectrum of patient-specific neoantigens and safe adjuvants and effectively activate tumor-reactive T cells. SCCNVs may show clinical benefit since SCCNVs showed an efficacy similar to that of immune checkpoint blockade therapy (anti-PD-L1 antibody) in our animal study (Fig. 7). Moreover, immune checkpoint inhibitors that prevent T-cell exhaustion in the immunosuppressive TME can function synergistically with tumor-reactive T cells activated by SCCNVs to inhibit tumor growth (Fig. 7). Therefore, we suggest SCCNVs as a novel personalized cancer vaccine with facile and simple procedures.

REFERENCES

- Waldman, A. D., Fritz, J. M. & Lenardo, M. J. A guide to cancer immunotherapy: from T cell basic science to clinical practice. *Nat. Rev. Immunol.* **20**, 651–668 (2020).
- Ghorashian, S. et al. Enhanced CAR T cell expansion and prolonged persistence in pediatric patients with ALL treated with a low-affinity CD19 CAR. *Nat. Med.* **25**, 1408–1414 (2019).
- Fry, T. J. et al. CD22-targeted CAR T cells induce remission in B-ALL that is naive or resistant to CD19-targeted CAR immunotherapy. *Nat. Med.* **24**, 20 (2018).
- Shin, S. et al. Tumor microenvironment modulating functional nanoparticles for effective cancer treatments. *Tissue Eng. Regen. Med.* **19**, 205–219 (2022).
- Morse, M. A., Gwin, W. R. & Mitchell, D. A. Vaccine therapies for cancer: then and now. *Target. Oncol.* **16**, 1–32 (2021).
- Cheever, M. A. & Higano, C. S. PROVENGE (Sipuleucel-T) in prostate cancer: the first FDA-approved therapeutic cancer vaccine. *Clin. Cancer Res.* **17**, 3520–3526 (2011).
- Ye, Z., Qian, Q., Jin, H. & Qian, Q. Cancer vaccine: learning lessons from immune checkpoint inhibitors. *J. Cancer* **9**, 263 (2018).
- Accolla, R. S., Buonaguro, L., Melief, C., Rammensee, H.-G. & Bassani-Sternberg, M. Novel strategies for anti-tumor vaccines. *Front. Immunol.* **10**, 3117 (2020).
- Buonaguro, L. & Tagliamonte, M. Selecting target antigens for cancer vaccine development. *Vaccines* **8**, 615 (2020).
- Peng, M. et al. Neoantigen vaccine: an emerging tumor immunotherapy. *Mol. Cancer* **18**, 1–14 (2019).
- Schumacher, T. N. & Schreiber, R. D. Neoantigens in cancer immunotherapy. *Science* **348**, 69–74 (2015).
- Bodey, B., Bodey, B. Jr, Siegel, S. E. & Kaiser, H. E. Failure of cancer vaccines: the significant limitations of this approach to immunotherapy. *Anticancer Res.* **20**, 2665–2676 (2000).
- Karpanen, T. & Olweus, J. The potential of donor T-cell repertoires in neoantigen-targeted cancer immunotherapy. *Front. Immunol.* **8**, 1718 (2017).
- Kaiser, J. Personalized tumor vaccines keep cancer in check. *Science* **356**, 6334 (2017).
- Rosenberg, S. A. & Restifo, N. P. Adoptive cell transfer as personalized immunotherapy for human cancer. *Science* **348**, 62–68 (2015).
- Kroll, A. V. et al. Nanoparticulate delivery of cancer cell membrane elicits multi-antigenic antitumor immunity. *Adv. Mater.* **29**, 1703969 (2017).
- Fang, R. H. et al. Cancer cell membrane-coated nanoparticles for anticancer vaccination and drug delivery. *Nano Lett.* **14**, 2181–2188 (2014).
- Bowen, W. S., Srivastava, A. K., Batra, L., Barsoumian, H. & Shirwan, H. Current challenges for cancer vaccine adjuvant development. *Expert Rev. Vaccines* **17**, 207–215 (2018).
- Banstola, A., Jeong, J.-H. & Yook, S. Immunoadjuvants for cancer immunotherapy: a review of recent developments. *Acta Biomater.* **114**, 16–30 (2020).
- Cuzzubbo, S. et al. Cancer vaccines: adjuvant potency, importance of age, life-style, and treatments. *Front. Immunol.* **11**, 3850 (2021).
- Link, B. K. et al. Oligodeoxynucleotide CpG 7909 delivered as intravenous infusion demonstrates immunologic modulation in patients with previously treated non-Hodgkin lymphoma. *J. Immunother.* **29**, 558–568 (2006).
- Dudek, A. Z. et al. First in human phase I trial of 852A, a novel systemic toll-like receptor 7 agonist, to activate innate immune responses in patients with advanced cancer. *Clin. Cancer Res.* **13**, 7119–7125 (2007).
- Jang, S. C. et al. Bioinspired exosome-mimetic nanovesicles for targeted delivery of chemotherapeutics to malignant tumors. *ACS nano* **7**, 7698–7710 (2013).
- Choo, Y. W. et al. M1 macrophage-derived nanovesicles potentiate the anticancer efficacy of immune checkpoint inhibitors. *ACS Nano* **12**, 8977–8993 (2018).
- Hong, J. et al. T-cell-derived nanovesicles for cancer immunotherapy. *Adv. Mater.* **33**, 2101110 (2021).
- Jung, M. et al. Nanovesicle-mediated targeted delivery of immune checkpoint blockades to potentiate therapeutic efficacy and prevent side effects. *Adv. Mater.* **34**, 2106516 (2022).
- Van Deursen, J. M. The role of senescent cells in ageing. *Nature* **509**, 439–446 (2014).
- Crescenzi, E. et al. NF- κ B-dependent cytokine secretion controls Fas expression on chemotherapy-induced premature senescent tumor cells. *Oncogene* **30**, 2707–2717 (2011).
- Liu, H. et al. Functional crosstalk between mTORC1/p70S6K pathway and heterochromatin organization in stress-induced senescence of MSCs. *Stem Cell Res. Ther.* **11**, 1–17 (2020).
- Hsu, C.-H., Altschuler, S. J. & Wu, L. F. Patterns of early p21 dynamics determine proliferation-senescence cell fate after chemotherapy. *Cell* **178**, 361–373.e312 (2019).
- Hsu, D.-H. et al. Exosomes as a tumor vaccine: enhancing potency through direct loading of antigenic peptides. *J. Immunother.* **26**, 440–450 (2003).
- Admyre, C., Johansson, S. M., Paulie, S. & Gabriellson, S. Direct exosome stimulation of peripheral human T cells detected by ELISPOT. *Eur. J. Immunol.* **36**, 1772–1781 (2006).
- Kim, H. Y. et al. Immunomodulatory lipocomplex functionalized with photosensitizer-embedded cancer cell membrane inhibits tumor growth and metastasis. *Nano Lett.* **19**, 5185–5193 (2019).
- Schlickeiser, S. et al. Control of TNF-induced dendritic cell maturation by hybrid-type N-glycans. *J. Immunol.* **186**, 5201–5211 (2011).
- Gardner, J. K. et al. Elderly dendritic cells respond to LPS/IFN- γ and CD40L stimulation despite incomplete maturation. *PLoS One* **13**, e0195313 (2018).
- Kang, M. et al. T-cell-mimicking nanoparticles for cancer immunotherapy. *Adv. Mater.* **32**, 2003368 (2020).
- Kang, M. et al. Nanocomplex-mediated in vivo programming to chimeric antigen receptor-M1 macrophages for cancer therapy. *Adv. Mater.* **33**, 2103258 (2021).
- Reddy, S. T. et al. Exploiting lymphatic transport and complement activation in nanoparticle vaccines. *Nat. Biotechnol.* **25**, 1159–1164 (2007).
- Schudel, A., Francis, D. M. & Thomas, S. N. Material design for lymph node drug delivery. *Nat. Rev. Mater.* **4**, 415–428 (2019).
- Swartz, M. A. The physiology of the lymphatic system. *Adv. Drug Deliv. Rev.* **50**, 3–20 (2001).
- Whiteside, T. L. Tumor-derived exosomes and their role in cancer progression. *Adv. Clin. Chem.* **74**, 103–141 (2016).
- Kim, H. Y. et al. Therapeutic efficacy-potentiated and diseased organ-targeting nanovesicles derived from mesenchymal stem cells for spinal cord injury treatment. *Nano Lett.* **18**, 4965–4975 (2018).
- Gu, X., Erb, U., Büchler, M. W. & Zöller, M. Improved vaccine efficacy of tumor exosome compared to tumor lysate loaded dendritic cells in mice. *Int. J. Cancer* **136**, E74–E84 (2015).
- Kersten, K., de Visser, K. E., van Miltenburg, M. H. & Jonkers, J. Genetically engineered mouse models in oncology research and cancer medicine. *EMBO Mol. Med.* **9**, 137–153 (2017).
- Mardiana, S. & Gill, S. CAR T cells for acute myeloid leukemia: state of the art and future directions. *Front. Oncol.* **10**, 697 (2020).
- Jimbu, L. et al. Is there a place for PD-1/PD-L blockade in acute myeloid leukemia? *Pharmaceuticals* **14**, 288 (2021).
- Liu, C. et al. A nanovaccine for antigen self-presentation and immunosuppression reversal as a personalized cancer immunotherapy strategy. *Nat. Nanotechnol.* **17**, 531–540 (2022).

ACKNOWLEDGEMENTS

All animal experiments were approved by the Institutional Animal Care and Use Committee (IACUC) of Seoul National University (SNU-200630-2-4) and performed in

compliance with the guidelines of the IACUC. This study was supported by a grant (2019M3A9H1103651) from the National Research Foundation of Korea.

COMPETING INTERESTS

The authors declare no competing interests.

ADDITIONAL INFORMATION

Supplementary information The online version contains supplementary material available at <https://doi.org/10.1038/s12276-023-00951-z>.

Correspondence and requests for materials should be addressed to Byung-Soo Kim.

Reprints and permission information is available at <http://www.nature.com/reprints>

Publisher's note Springer Nature remains neutral with regard to jurisdictional claims in published maps and institutional affiliations.



Open Access This article is licensed under a Creative Commons Attribution 4.0 International License, which permits use, sharing, adaptation, distribution and reproduction in any medium or format, as long as you give appropriate credit to the original author(s) and the source, provide a link to the Creative Commons license, and indicate if changes were made. The images or other third party material in this article are included in the article's Creative Commons license, unless indicated otherwise in a credit line to the material. If material is not included in the article's Creative Commons license and your intended use is not permitted by statutory regulation or exceeds the permitted use, you will need to obtain permission directly from the copyright holder. To view a copy of this license, visit <http://creativecommons.org/licenses/by/4.0/>.

© The Author(s) 2023